MATERIALS SCIENCE

Proton-conductive aromatic membranes reinforced with poly(vinylidene fluoride) nanofibers for high-performance durable fuel cells

Fanghua Liu[1,2], Ick S. Kim[3], Kenji Miyatake[1,4,5]*

Durability and ion conductivity are counteracting properties of proton-conductive membranes that are challenging to achieve simultaneously and determine the lifetime and performance of proton exchange membrane fuel cells. Here, we developed aromatic ionomers reinforced with nonwoven poly(vinylidene fluoride) (PVDF) nanofibers. Because of the right combination of an isotropic nonwoven PVDF with high porosity (78%) and partially fluorinated aromatic ionomers (SPP-TFP-4.0), the resulting composite membrane (SPP-TFP-4.0-PVDF) outperformed state-of-the-art chemically stabilized and physically reinforced perfluorinated Nafion XL membrane, in terms of fuel cell operation and in situ chemical stability at a high temperature (120°C) and low relative humidity (30%). The SPP-TFP-4.0-PVDF membrane exhibited excellent chemical stability and stable rupture energy at high and low RH levels, allowing it to be an alternative proton-conductive membrane to meet the U.S. Department of Energy target to be used in automobile fuel cells in 2025.

INTRODUCTION

Proton exchange membrane fuel cells (PEMFCs) have been used commercially in electric vehicles and stationary cogeneration systems for the last decade, and they are expected to play pivotal roles in realizing a hydrogen-based, carbon-free society (*1*–*5*). PEMFCs must have long-term durability to adapt to transient variations such as temperature and humidity and further gain competitiveness in the market. For this purpose, the U.S. Department of Energy (DOE) has established highly challenging technical targets for each constituent material. For example, by 2025, PEMs must pass an accelerated durability test (ADT) or a combined chemical and mechanical test that simulates heavily loaded conditions for more than 20,000 cycles with a <20% loss in an open-circuit voltage (OCV) (*6*). The chemical test involves holding the OCV to accelerate free radical generation, while the mechanical test involves humidity cycling to accelerate the formation and growth of membrane cracks and holes.

The durability issues of PEMs are difficult to address because chemical and mechanical degradations are not independent but rather synergistically related. Polymer chain decomposition induces membrane fragility and mechanical failure, which enhance hydrogen/oxygen crossover and eventually cause oxidative polymer degradation (*7*–*10*). State-of-the-art PEMs that are used in commercial PEMFCs are perfluorosulfonic acid (PFSA) polymer membranes stabilized with antioxidative additives (such as CeO_2) and reinforced with porous expanded polytetrafluoroethylene (ePTFE) (*11*–*15*). These chemically and physically modified PFSA membranes, such as Nafion HP, Nafion XL, and Gore-Select, have proven to be much more durable than unmodified PFSA membranes in fuel cell operations (*16*–*20*). The mechanism underlying their increased durability has also been investigated (*21*–*27*). In a previous study, Nafion XL membranes exhibited outstanding durability in a humidity cycle test for >20,000 cycles, but they achieved only 9,900 cycles in the combined durability test (the abovementioned DOE protocol), presumably because they underwent chemical degradation under such severe conditions (*28*).

Sulfonated polyphenylenes (SPPs) have been extensively investigated as promising alternatives because of the inherent chemical and thermal stabilities of aromatic polymers free from heteroatom linkages in their main chain (*29*–*32*). Some SPP-based membranes have been reported to exhibit higher proton conductivity and comparable or better fuel cell performance than PFSA and stabilized/reinforced PFSA membranes (*33*, *34*). However, SPP-based membranes must have a high sulfonic acid concentration [or ion exchange capacity (IEC)] to function as PEMs, which eventually results in high water uptake, swelling, and mechanical instability (*35*). Therefore, it is challenging to commercialize SPP-based membranes in terms of longevity. Holdcroft and colleagues reported a method for reducing swelling via acid-base interactions and preventing substantial proton conductivity loss by incorporating sterically hindered triphenylated phenyl (TPPy) containing N-heterocycle groups into SPPs (STPPyPPs) (*36*). The incorporation of the heterocycle groups exhibited a remarkable effect on improving the mechanical stability and robustness, but it compromised the fuel cell performance. Our group proposed another effective method for improving the mechanical properties of SPP-based membranes via physical reinforcement (*37*). We embedded a porous polyethylene substrate into an SPP ionomer to form homogeneous composite membranes (SPP-QP-PE). Although the membranes exhibited better mechanical stability (negligible hydrogen crossover after 3,850 humidity cycles) than its parent SPP-QP membrane, their cyclability remained unsatisfactory. They also exhibited slightly lower fuel cell performance than the parent SPP-QP membrane and the reinforced PFSA membranes. Pintauro and colleagues soaked a porous ePTFE film in a methanol solution of

[1]Clean Energy Research Center, University of Yamanashi, 4-4-37 Takeda, Kofu, Yamanashi 400-8510, Japan. [2]Research Organization for Nano and Life Innovation, Waseda University, Tokyo 169-8555, Japan. [3]Nano Fusion Technology Research Group, Institute for Fiber Engineering, Interdisciplinary Cluster for Cutting Edge Research, Shinshu University, Nagano 380-8553, Japan. [4]Fuel Cell Nanomaterials Center, University of Yamanashi, 4-4-37 Takeda, Kofu, Yamanashi 400-8510, Japan. [5]Department of Applied Chemistry, and Research Institute for Science and Engineering, Waseda University, Tokyo 169-8555, Japan.
*Corresponding author. Email: miyatake@yamanashi.ac.jp

poly(phenylenesulfonic acid) (cPPSA), and then cross-linked the cPPSA ionomers inside of ePTFE pores to obtain composite cPPSA-ePTFE membrane (PFM) (*38*). The membrane outperformed Nafion XL in terms of proton conductivity (47.5 mS cm^{-1} of PFM versus 13.6 mS cm^{-1} of Nafion XL at 80°C and 40% RH) and maximum power density (452 mW cm^{-2} of PFM and 211 mW cm^{-2} of Nafion XL at 80°C and 30% RH). Although the membrane was reinforced and cross-linked, high water uptake (26% at 80°C and 40% RH), low maximum strain (less than 18% at 25°C and 50% RH), and low chemical stability (2 mW cm^{-2} $hour^{-1}$ decay rate) need improvement. In a previous study, SPP-TP-f-DPTFE, our originally designed composite membrane that contains vertically aligned double-layered ePTFE sheets, exhibited higher fuel cell performance than unstabilized Nafion NRE 211 membranes at a wide temperature range (*39*). However, SPP-TP-f-DPTFE lasted for only 2300 cycles in the abovementioned DOE protocol. The achieved life span did not threaten state-of-the-art stabilized/reinforced PFSA membranes. To the best of our knowledge, none of the existing alternative PEMs have fulfilled the DOE target, probably because of a lack of suitable chemical and/or physical reinforcement techniques (*40*). Moreover, there are not many types of commercially available ePTFE.

Electrospinning is a useful technique for preparing nanofibers using various polymers and fabricating nonwoven thin films with more easily controllable properties, such as porosity, pore size, fiber diameter, thickness, wettability, and mechanical strength, than traditional expanded porous materials (*41*–*43*). Application of the nanofibrous materials fabricated by electrospinning for energy conversions and storage devices has attracted great attention (*44*–*46*). Kim and colleagues developed a series of electrospun poly(vinylidene fluoride) (PVDF) nanofiber fabrics and optimized the microstructures for a lithium-ion battery separator (*47*). The resulting composite separators contributed to prolonging the lifetime of the lithium-ion batteries. Hoorfar and colleagues impregnated Nafion solution to electrospun PVDF nanofibers to fabricate Nafion/PVDF composite membranes, which performed better than Nafion membrane in dimensional stability and direct methanol fuel cells where PVDF functioned as an efficient methanol barrier (*48*). Pintauro and colleagues reported a homogenous electrospun PVDF/Nafion membrane by hot-pressing (*49*). It exhibited a 46% higher maximum power density than that of the Nafion 212 membrane in an H_2/Br_2 regenerative fuel cell. These findings inspired us to adopt electrospun PVDF nanofiber films as the reinforcement substrates for SPP ionomer membranes.

Therefore, we fabricated an electrospun PVDF nanofiber fabric with a high porosity (78%), a large pore size (0.28 μm), a small thickness (7 μm), and isotropic mechanical properties specifically tailored for PEMs and redesigned SPP ionomers (SPP-TFP; Fig. 1A) (*50*) with high affinity for the PVDF nanofiber fabrics. SPP-TFP had structural characteristics such as a high local concentration of CF_3 groups (two CF_3 groups were located on a single phenylene ring in the terphenylene groups) and a high sulfonic acid density (the target and titrated IECs were 4.0 and 3.4 mmol g^{-1}, respectively). A single PVDF sheet was sufficient to create a composite membrane with a satisfactory reinforcement effect because of its (vertically and horizontally) isotropic high mechanical strength. The tuned combination of SPP-TFP-4.0 and nonwoven PVDF fabric provided the resulting composite membrane with high robustness without compromising proton conductivity and even fuel cell performance. This paper discusses the origin of the outstanding reinforcement effect of SPP-TFP-4.0-PVDF and presents a thorough comparison of the fabricated membranes with commercial state-of-the-art PFSA membranes (Nafion XL and NRE 211) in terms of membrane properties, fuel cell performance, and durability.

RESULTS

Preparation of the reinforced SPP-TFP-4.0-PVDF and SPP-TFP-4.0-ePTFE membranes

The SPP-TFP-4.0 ionomer (target IEC = 4.0 mmol g^{-1}) was synthesized using our previously reported method (*50*). The ionomer was soluble in polar aprotic solvents [e.g., dimethyl sulfoxide (DMSO)] and lower alcohols (ethanol, isopropanol, etc.). The contact angles of some solvents (DMSO, dimethylacetamide (DMAc), ethanol, and isopropanol) on the porous nonwoven PVDF nanofiber fabric (Fig. 1B) and ePTFE (Fig. 1C) substrate were summarized (fig. S1). PVDF was observed to have substantially lower contact angles than ePTFE with any solvent. In particular, isopropanol had an affinity for porous materials with small contact angles: 4.9° for PVDF and 21.6° for ePTFE (Fig. 1D). Therefore, a push-coating method was used to prepare the composite (reinforced) membranes, SPP-TFP-4.0-PVDF and SPP-TFP-4.0-ePTFE, by applying an SPP-TFP-4.0 ionomer-containing isopropanol solution to the porous nonwoven PVDF fabric (fig. S2A) or ePTFE substrate (fig. S2B). Transparent, pale brown, homogeneous, and bendable reinforced membranes were obtained after evaporating the solvent at 25°C using a silicon sheet (fig. S2, C and D). SPP-TFP-4.0-PVDF and SPP-TFP-4.0-ePTFE had somewhat larger thicknesses (14 and 16 μm, respectively) than the parent porous materials (7 and 11 μm, respectively).

Morphology of the reinforced membranes

The reinforced membranes were analyzed using cross-sectional scanning electron microscopy (SEM; Fig. 1, E and F). The porous nonwoven PVDF fabric and porous ePTFE substrate were both impregnated effectively with the ionomers without detectable defects (e.g., pores or cracks). The sandwich-like structure was observed more clearly in SPP-TFP-4.0-ePTFE than in SPP-TFP-4.0-PVDF, probably because of the better compatibility of SPP-TFP-4.0-isopropanol solution with porous nonwoven PVDF fabric than with ePTFE substrate. Energy-dispersive x-ray spectroscopy (EDS) elemental mapping confirmed the triple-layer structure of the reinforced membranes in which the middle layer contained the fluorinated substrates (7 μm for SPP-TFP-4.0-PVDF and 9 μm for SPP-TFP-4.0-ePTFE) (fig. S3). The top layer (2 μm for SPP-TFP-4.0-PVDF and 2 μm for SPP-TFP-4.0-ePTFE) and the bottom layer (7 μm for SPP-TFP-4.0-PVDF and 7 μm for SPP-TFP-4.0-ePTFE) consisted solely of the SPP-TFP-4.0 ionomer. The total membrane thickness confirmed by the cross-sectional SEM images agreed with the micrometer measurement.

Transmission electron microscopy (TEM) images were collected to analyze the hydrophilic/hydrophobic phase-separated morphology of the ionomer in the reinforced membranes. The hydrophilic domains with aggregated sulfonic acid groups appeared as dark areas in the TEM images (Fig. 1, G to I). The ionomer in the porous materials exhibited phase separation similar to that of the parent SPP-TFP-4.0 membrane (Fig. 1G) (*50*), while the interfaces

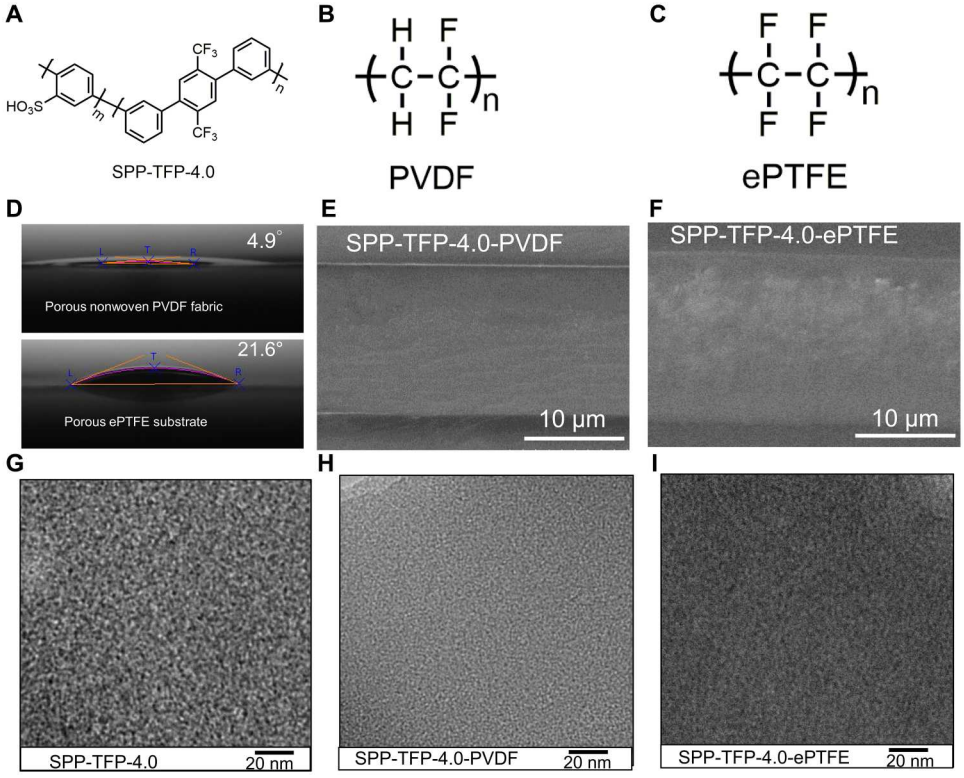

Fig. 1. Chemical structure, cross-sectional SEM images, and TEM images of membranes. (**A**) Chemical structure of SPP-TFP-4.0. (**B**) Chemical structure of PVDF. (**C**) Chemical structure of ePTFE. (**D**) Contact angles of the isopropanol droplet on the porous nonwoven PVDF fabric and porous ePTFE substrate at room temperature. (**E**) Cross-sectional scanning electron microscopy (SEM) image of reinforced SPP-TFP-4.0-PVDF membrane. (**F**) Cross-sectional SEM image of reinforced SPP-TFP-4.0-ePTFE membrane. (**G**) Transmission electron microscopy (TEM) image of their parent SPP-TFP-4.0 membrane (*50*). (**H**) TEM image of reinforced SPP-TFP-4.0-PVDF membrane. (**I**) TEM image of reinforced SPP-TFP-4.0-ePTFE membrane. SEM images of the membranes were obtained at an accelerating voltage of 15.0 kV. TEM images were obtained at an accelerating voltage of 200 kV.

of the hydrophilic and hydrophobic clusters became less distinct in the reinforced membranes. SPP-TFP-4.0-PVDF and SPP-TFP-4.0-ePTFE had hydrophilic domain sizes (average diameter: ≥70 spots) of 1.11 ± 0.24 nm and 1.74 ± 0.33 nm, respectively, which were smaller than that of the parent SPP-TFP-4.0 membrane (2.50 ± 0.30 nm). However, SPP-TFP-4.0-PVDF and SPP-TFP-4.0-ePTFE had hydrophobic domain sizes of 1.84 ± 0.15 nm and 1.93 ± 0.27 nm, respectively, which were more comparable to that of the parent SPP-TFP-4.0 membrane (1.70 ± 0.20 nm). Although the pore sizes of PVDF and ePTFE (0.28 and 0.4 to 0.7 μm, respectively) were substantially larger than the hydrophilic/hydrophobic clusters, the phase separation in the reinforced membranes appeared to be somewhat suppressed.

Water uptake and proton conductivity

The IECs of the reinforced SPP-TFP-4.0-PVDF and SPP-TFP-4.0-ePTFE membranes were calculated to be 2.96 and 2.95 mmol g^{-1}, respectively, on the basis of the thickness of each layer in the SEM images and the titrated IEC of the parent SPP-TFP-4.0 membrane. The titrated IECs of the reinforced membranes (table S1) were lower than the calculated IECs, indicating that the H^+ of the ionomer filled in the pores of the porous substrates was not exchanged completely even in 2 M NaCl aqueous solution at 50°C for 48 hours. SPP-TFP-4.0-PVDF had a slightly lower titrated IEC (2.01 mmol g^{-1}) than SPP-TFP-4.0-ePTFE (2.13 mmol g^{-1}), indicating that ion exchange became less efficient as the pore sizes decreased.

The water uptake and proton conductivity of the membrane were measured at 80°C and plotted as functions of the relative humidity (RH; Fig. 2, A and B). The membranes exhibited RH-dependent water uptake. The water uptake was in the order of the IEC. Despite their minor differences in IECs, SPP-TFP-4.0-PVDF absorbed substantially less water than SPP-TFP-4.0-ePTFE. This was further demonstrated by their enhanced dimensional stability in water, which was 5.1% (in-plane) and 6.3% (through-plane) for SPP-TFP-4.0-PVDF and 13.5% (in-plane) and 14.3% (through-plane) for SPP-TFP-4.0-ePTFE (Fig. 2C). (Note that both reinforced membranes exhibited isotropic in-plane swelling.) It is noteworthy that SPP-TFP-4.0-PVDF exhibited considerably less swelling than Nafion NRE 211 and comparable swelling to reinforced Nafion XL, with smaller IECs in both (in-plane and through-plane) directions.

The proton conductivity of the membranes was measured under the same conditions as the water uptake (Fig. 2B). It was reasonable that all the reinforced membranes exhibited lower water uptake and proton conductivity than their corresponding parent polymer membranes. At any RH level, the parent SPP-TFP-4.0 membrane exhibited the highest conductivity because it had the highest IEC. For example, at 95% RH, SPP-TFP-4.0-PVDF and SPP-TFP-4.0-ePTFE had proton conductivities of 281.8 and 387.5 mS cm^{-1},

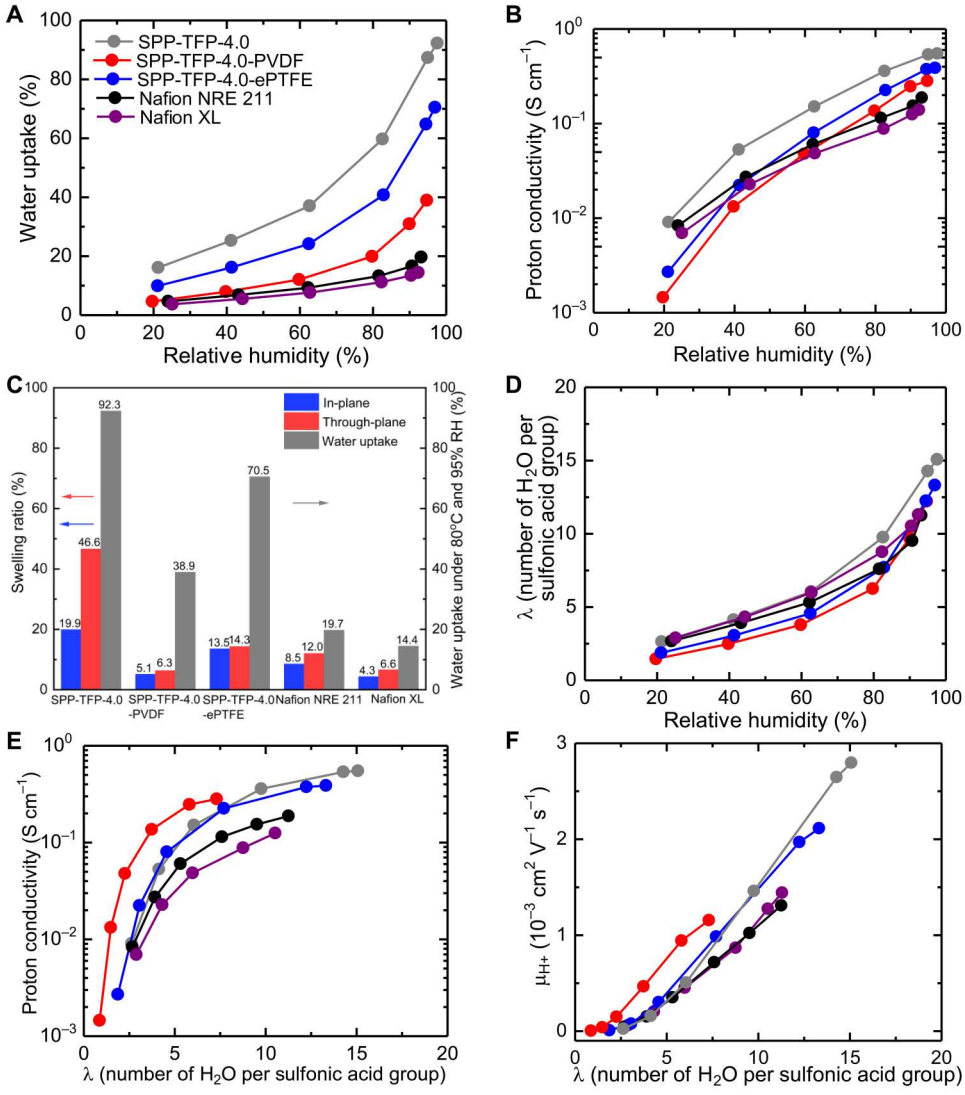

Fig. 2. Dimensional change and proton conductivity. (**A**) Water uptake as a function of RH at 80°C. (**B**) Proton conductivity as a function of RH at 80°C. (**C**) Swelling ratio at room temperature and under fully hydrated conditions, and water uptake at 80°C and 95% RH. (**D**) The λ (number of absorbed water molecules per sulfonic acid group) as a function of RH. (**E**) Proton conductivity as a function of λ. (**F**) The proton mobility (μ_{H+}) as a function of λ.

respectively, whereas the parent SPP-TFP-4.0 membrane had a conductivity of 550.1 mS cm^{-1}. Similar to the water uptake case, SPP-TFP-4.0-ePTFE with a higher titrated IEC (2.13 mmol g^{-1}) had a higher proton conductivity than SPP-TFP-4.0-PVDF (titrated IEC: 2.01 mmol g^{-1}) at any RH level. The proton conductivity is replotted as a function of λ (number of absorbed water molecules per sulfonic acid group) to provide a more quantitative explanation (Fig. 2E). Despite having different IEC values, SPP-TFP-4.0 and the reinforced membranes exhibited similar proton conductivities when the λ value was high (λ > 7). This is presumably because the Grotthuss mechanism (proton hopping via hydrogen bonds between water molecules and hydronium ions) was dominant. However, the proton conductivity was in the following order when the λ value was low (λ ≤ 7); SPP-TFP-4.0-PVDF > SPP-TFP-4.0-ePTFE ≥ SPP-TFP-4.0. This trend became more pronounced as the λ value decreased. From the water uptake dependence of the proton conductivity (fig. S4), SPP-TFP-4.0-PVDF showed higher proton conductivity than SPP-TFP-4.0 and SPP-TFP-4.0-ePTFE at the same water uptake level. These results imply that the SPP-TFP-4.0 ionomer used water molecules for proton conduction more efficiently with the PVDF fabric than with the ePTFE substrate, which was proved through the increased hydronium ion or proton mobility (Fig. 2F) in SPP-TFP-4.0-PVDF membrane. Choosing a suitable reinforcement material was crucial for mitigating the RH (or water uptake) dependence of the proton conductivity. The water uptake and proton conductivity of the reinforced membranes are normalized with those of the parent SPP-TFP-4.0 (fig. S5). It was found that SPP-TFP-4.0-PVDF had a considerably higher decrease in water uptake than SPP-TFP-4.0-ePTFE and indicated that porous PVDF fabric, not ePTFE substrate, increased water utilization for proton conduction.

Mechanical properties

The tensile and viscoelastic properties were measured to investigate the effect of porous substrates on the mechanical properties of the reinforced membranes. The tensile properties were evaluated at 80°C under high (60%) and low (0%) RH levels (Fig. 3, A and B). For reference, the tensile properties of the ePTFE substrate in the machine direction (MD) and the PVDF fabric at 60% RH were measured, where the tensile properties for the porous ePTFE substrate along the transverse direction (TD) could not be obtained (fig. S6). The results are summarized in Table 1 (data for Nafion NRE 211 and Nafion XL are also provided for reference). The parent and reinforced membranes exhibited a higher strain, lower stress, and lower Young's modulus at 60% RH than at 0% RH because the absorbed water functioned as a plasticizer (*51*, *52*). SPP-TFP-4.0-ePTFE and Nafion XL exhibited larger stress and smaller strain in the MD than in the TD, while the SPP-TFP-4.0-PVDF membrane had isotropic stress and strain properties. At 0% RH, SPP-TFP-4.0-PVDF exhibited a higher maximum strain (39.7%) than the parent SPP-TFP-4.0 (20.8%) and SPP-TFP-4.0-ePTFE (MD: 15.3% and TD: 31.5%) membranes. The SPP-TFP-4.0-PVDF and parent SPP-TFP-4.0 membranes exhibited comparably higher maximum stress (85.5 and 95.0 MPa, respectively) than SPP-TFP-4.0-ePTFE (MD: 22.9 MPa and TD: 11.3 MPa). A single PVDF fabric clearly provided more sufficient reinforcement effects than a single ePTFE substrate. At 60% RH, all the parent and reinforced membranes had maximum strains of >100% and the parent SPP-TFP-4.0 membrane exhibited the highest maximum stress and strain followed by SPP-TFP-4.0-PVDF. Similarly, the reinforced Nafion XL membrane exhibited a smaller maximum strain than Nafion NRE 211.

Thereafter, the rupture energies were calculated and plotted as a function of the RH (Fig. 3C; see Table 1 for details). The rupture energy of the parent SPP-TFP-4.0 membrane increased substantially with a 236.4% increase as the RH increased from 0 to 60%. The SPP-TFP-4.0-ePTFE membrane exhibited more conspicuous and anisotropic behavior in terms of rupture energy (834.6 and 496.4% increases in the MD and TD, respectively). SPP-TFP-4.0-PVDF exhibited rupture energy that was much less sensitive to the RH, with only a 3.3% increase from 0 to 60% RH. This was because it had a lower water uptake and swelling ratio than the parent SPP-TFP-4.0 and SPP-TFP-4.0-ePTFE membranes (Fig. 2, A and C). Nafion XL also exhibited a small change in rupture energy in the same direction (4.7% increase and 5.8% decrease in the MD and TD, respectively) as the RH changed; however, its rupture energy exhibited anisotropic behavior between the MD and TD. Nafion NRE 211 exhibited rupture energy that was negatively dependent on the RH (−39.6%). A possible explanation for the opposite change in rupture energy with RH is related to the different effects of water on polyphenylene-based and perfluoroalkyl-based ionomer membranes. For the polyphenylene-based membranes (SPP-TFP-4.0 and its reinforced membranes), the absorbed water affects more on the strain than the stress due to the inherent rigidity of the polyphenylene structures. From 60 to 0% RH, SPP-TFP-4.0-PVDF showed a 241% increase in yield stress and a 318% decrease in maximum strain. In contrast, the absorbed water affects more on the stress than the strain for the perfluoroalkylated membranes. Nafion XL-TD showed a 130% increase in yield stress and a 115% decrease in maximum strain. Nafion XL-MD showed a similar trend.

The viscoelastic properties of the parent and reinforced membranes were evaluated using dynamic mechanical analysis under two different conditions: variable RH at a constant temperature (80°C) and variable temperatures at constant RH (60%) (fig. S7), simulating various fuel cell conditions. At 80°C, the storage modulus (E′) decreased as the RH increased and was in the following order: parent SPP-TFP-4.0 > SPP-TFP-4.0-PVDF > SPP-TFP-4.0-ePTFE. In the E″ curves, the parent SPP-TFP-4.0 and SPP-TFP-4.0-PVDF membranes exhibited a broad (but not prominent) peak at ca. 10% RH, while the SPP-TFP-4.0-ePTFE membrane exhibited a similar peak at ca. 30 to 40% RH. The peak is attributed to the glass transition of the ionomer, and the micro-Brownian motion of SPP-TFP-4.0 may have been restricted in the pores of the ePTFE substrate. At 60% RH, compared to the Nafion NRE 211 and Nafion XL membranes, which exhibited broad and minor glass transition peaks at ca. 80°C in the E″ curves (fig. S7E), SPP-TFP-4.0 and the reinforced membranes were more thermally stable under the same temperature and RH conditions.

Fuel cell performance

Catalyst-coated membranes (CCMs) were prepared and assembled in fuel cells to evaluate the hydrogen permeability and fuel cell performance of the membranes. After conditioning, the cyclic

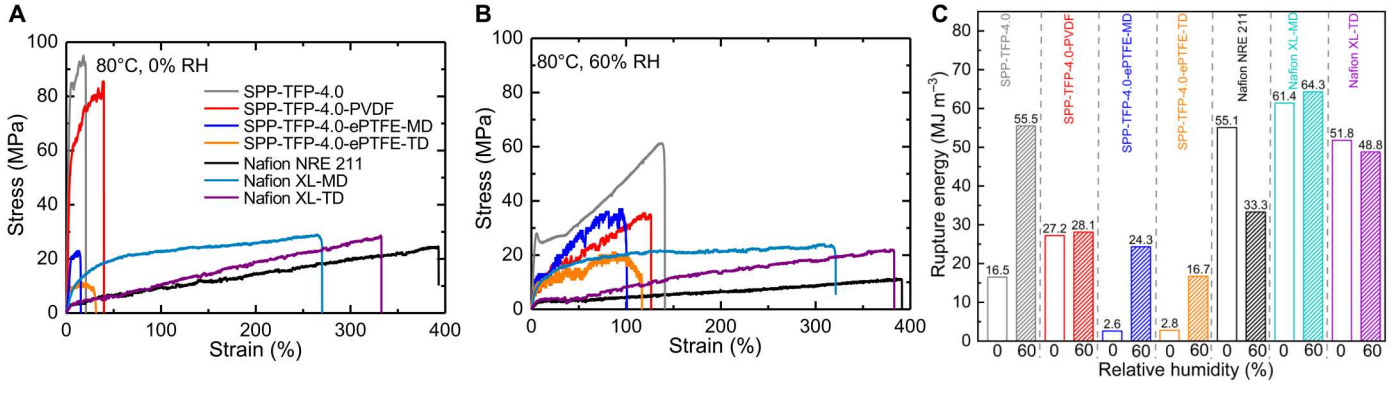

Fig. 3. Mechanical properties at 80°C and 0 and 60% RH. Tensile properties of SPP-TFP-4.0-ePTFE and Nafion XL in the different directions, SPP-TFP-4.0-PVDF, parent SPP-TFP-4.0, and Nafion NRE 211 at 0 (**A**) and 60% RH (**B**). (**C**) Rupture energy of SPP-TFP-4.0-ePTFE and Nafion XL in the different directions, SPP-TFP-4.0-PVDF, parent SPP-TFP-4.0, and Nafion NRE 211 as a function of RH.

Table 1. Summary of the mechanical properties and rupture energy of membranes at 80°C and 0 and 60% RH. ×, could not be obtained; –, was not measured.

Membrane	Yield stress (MPa)		Maximum strain (%)		Young's modulus (GPa)		Rupture energy (MJ m^{-3})		Change of rupture energy (%)
	0% RH	60% RH	0% RH	60% RH	0% RH	60% RH	0% RH	60% RH	
SPP-TFP-4.0	95.0	61.3	20.8	141.0	1.96	0.54	16.5	55.5	+236.4
SPP-TFP-4.0-PVDF	85.5	35.5	39.7	126.4	1.32	0.50	27.2	28.1	+3.3
SPP-TFP-4.0-ePTFE-MD	22.9	37.0	15.3	100.8	0.39	0.25	2.6	24.3	+834.6
SPP-TFP-4.0-ePTFE-TD	11.3	21.0	31.5	116.7	0.48	0.31	2.8	16.7	+496.4
Nafion NRE 211	24.6	11.4	393.1	391.0	0.05	0.05	55.1	33.3	−39.6
Nafion XL-MD	29.0	24.0	270.1	321.2	0.12	0.16	61.4	64.3	+4.7
Nafion XL-TD	28.7	22.0	332.6	383.0	0.04	0.06	51.8	48.8	−5.8
pure PVDF	–	33.1	–	96.7	–	0.04	–	17.6	–
Pure ePTFE-MD	–	7.3	–	406.7	–	0.01	–	19.9	–
Pure ePTFE-TD	–	×	–	×	–	×	–	×	–

voltammetry (CV) was conducted at 40°C and 100% RH to determine the electrochemically active surface area (ECSA) of the membrane electrode assemblies (MEAs) (fig. S8). With the same electrodes, the reinforced membranes, in particular, SPP-TFP-4.0-PVDF, showed higher ECSA (80.7 and 72.1 $m^2\ g_{Pt}^{-1}$ for SPP-TFP-4.0-PVDF and -ePTFE, respectively) than parent SPP-TFP-4.0 (63.7 $m^2\ g^{-1}$). The linear sweep voltammograms (LSVs) of the cells at 80°C and 100% RH, with H_2 supply at the anode and N_2 supply at the cathode were shown in Fig. 4A. The reinforced SPP-TFP-4.0-PVDF and SPP-TFP-4.0-ePTFE membranes had slightly higher hydrogen crossover current densities (1.06 and 1.15 mA cm^{-2}, respectively) than the parent SPP-TFP-4.0 membrane (27 μm thick and 0.90 mA cm^{-2}). Notably, the reinforced membranes, including Nafion XL (30 μm thick and 1.07 mA cm^{-2}), had lower crossover currents than Nafion NRE 211 (25 μm thick and 1.27 mA cm^{-2}). Considering their small thicknesses (*53*), SPP-TFP-4.0-PVDF and SPP-TFP-4.0-ePTFE exhibited smaller hydrogen permeability than the other three membranes (table S2).

The fuel cell performance was first evaluated at 80°C (100% and 30% RH) and then at 100°C (53 and 30% RH) and 120°C (30% RH) without back pressure (Fig. 4, B to F, and fig. S9). Under all conditions, all membranes had OCV values higher than 0.97 V, reflecting their low hydrogen permeability, as demonstrated by the LSVs. At 80°C and 100% RH (Fig. 4C), the ohmic resistances (0.069, 0.065, and 0.101 ohm·cm^2 for SPP-TFP-4.0-PVDF, SPP-TFP-4.0, and SPP-TFP-4.0-ePTFE, respectively) were higher than that (0.005, 0.004, and 0.004 ohm·cm^2 for SPP-TFP-4.0-PVDF, SPP-TFP-4.0, and SPP-TFP-4.0-ePTFE, respectively) calculated from the proton conductivity and thickness (Fig. 4B), probably because of the contact resistance with the catalyst layer. The cell performance (cell voltage at the same current density) was in the order of SPP-TFP-4.0-PVDF ≥ SPP-TFP-4.0 > SPP-TFP-4.0-ePTFE. Because the catalyst layers were the same and the ohmic resistance was similar, the improved performance was attributable to the improved compatibility at the interface of the membrane and the catalyst layers. The Nyquist plots of electrochemical impedance spectra (EIS) (fig. S10) and IR-free polarization curves (fig. S11) further suggested the improved interfacial properties of SPP-TFP-4.0-PVDF and SPP-TFP-4.0, where the charge transfer resistance of SPP-TFP-4.0-PVDF was lower than that of SPP-TFP-4.0-ePTFE. This idea was also supported by the mass activity of Pt catalysts at 0.85 V (Fig. 4B), which was calculated on the basis of the Tafel curve (fig. S12) and Pt loading amount (0.5 mg cm^{-2}): 74.8, 58.9, and 59.7 A g_{Pt}^{-1} for SPP-TFP-4.0-PVDF, SPP-TFP-4.0, and SPP-TFP-4.0-ePTFE, respectively. While Nafion NRE 211 (187.9 mS cm^{-1}) had a higher proton conductivity than Nafion XL (139.5 mS cm^{-1}) at 95% RH, it had better compatibility with the catalyst layer, as suggested by their mass activities (133.4 and 110.7 A g_{Pt}^{-1} for Nafion NRE 211 and Nafion XL, respectively). Since OCV was low (0.84 V) at 80°C and 30% RH, the SPP-TFP-4.0-ePTFE cell was disassembled and several cracks were confirmed at the edge of SPP-TFP-4.0-ePTFE CCM. Therefore, the fuel cell test could not be continued. At 80°C and 30% RH (fig. S9A), the reinforced SPP-TFP-4.0-PVDF and parent SPP-TFP-4.0 membranes exhibited comparable current-voltage (*I-V*) performance because of their similar ohmic resistances (0.309 and 0.275 ohm·cm^2, respectively). However, Nafion XL exhibited inferior performance mostly because it had the highest ohmic resistance (0.557 ohm·cm^2). The ohmic resistance decreased as the current density increased because the back diffusion of generated water from the cathode moisturized the membranes. However, the effect of the back-diffused water diminished at 100° and 120°C (Fig. 4, E and F), because the generated water at the cathode tended to be discharged as a vapor from the outlet. In addition, a reduced fraction of liquid water and reduced oxygen partial pressure at higher temperatures should cause higher ohmic resistance and lower cathode performance, both contributing to the decreased performance (*54*). Under such harsh conditions, SPP-TFP-4.0 and the reinforced SPP-TFP-4.0-PVDF membrane both outperformed Nafion NRE 211 and Nafion XL at 100° and 120°C and at any humidity, demonstrating their superiority at high temperatures and a wide RH range. SPP-TFP-4.0, SPP-TFP-4.0-PVDF, Nafion NRE 211, and Nafion XL had maximum power densities of 245.9, 236.8, 166.9, and 162.3 mW cm^{-2}, respectively, at 120°C and 30% RH. In addition to high proton conductivity and good interfacial compatibility of SPP-TFP-4.0, nonwoven PVDF fabric as a suitable substrate for it

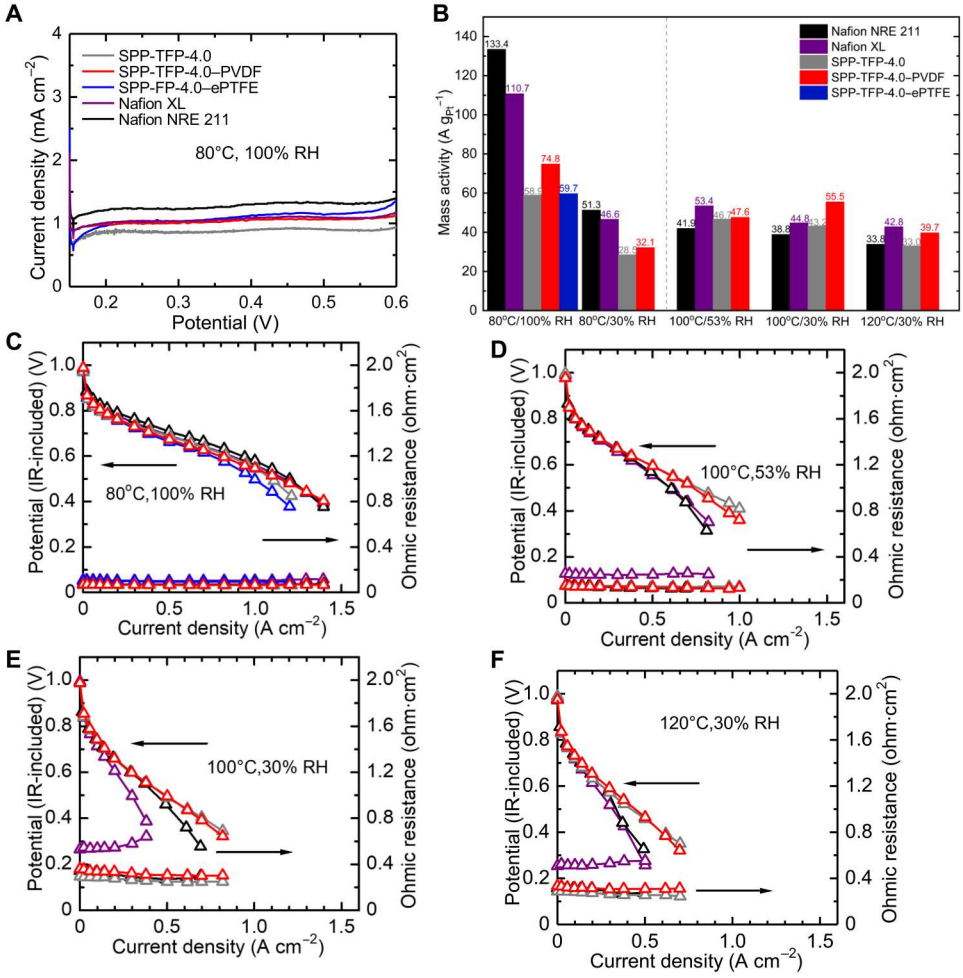

Fig. 4. LSV, the mass activity of Pt at 0.85 V, and IR-included polarization curves. (**A**) LSV of all cells at 80°C and 100% RH sweeping potential from 0.15 to 0.6 V at a scan rate of 0.5 mV s^{-1} and supplying hydrogen (0.1 slpm, anode) and nitrogen (0.1slpm, cathode). (**B**) Mass activity of Pt at 0.85 V under 80°C (100 and 30% RH), 100°C (53 and 30% RH), and 120°C (30% RH). IR-included polarization curves at 80°C and 100% RH (**C**), 100°C and 53% RH (**D**), 100°C and 30% RH (**E**), and 120°C and 30% RH (**F**). For the mass activity and IR-included polarization curves, the catalyst loading was 0.5 mg cm^{-2} for all electrodes supplying hydrogen and air to the anode and cathode, respectively, with no back pressure.

helped improve the mass activity of the Pt catalyst compared to the parent SPP-TFP-4.0 membrane, particularly at high temperatures and low RH levels (Fig. 4B). Similarly, Nafion XL showed higher mass activity of the Pt catalyst than Nafion NRE 211 at high temperatures.

Stability at 0.2 A cm^{-2}, 120°C, and 30% RH

The in situ chemical stability of the membranes was evaluated during fuel cell operations at a high temperature (120°C) and a low RH level (30%) at a constant current density (0.2 A cm^{-2}) for 600 hours (Fig. 5). Under such severe conditions, membranes are known to be considerably attacked by hydroxy and hydroperoxy radicals, which are products of crossed-over hydrogen, resulting in the rapid degradation of the membranes and a drop in the cell voltage (*55*). All membranes except for SPP-TFP-4.0-ePTFE were tested. Figure 5 shows that SPP-TFP-4.0-PVDF exhibited a slightly larger decrease in cell voltage from initial 0.631 V to final 0.581 V with an 83.3 μV $hour^{-1}$ average decay than parent SPP-TFP-4.0, which exhibited a cell voltage decrease from 0.638 to 0.605 V with a 55.0 μV $hour^{-1}$ average decay. This is presumably because the former was a thinner membrane (14 μm thick) with a slightly higher hydrogen crossover current (1.06 mA cm^{-2}) than the latter (27 μm thick and 0.90 mA cm^{-2}). Similarly, because of its larger hydrogen crossover, Nafion NRE 211 exhibited a slightly larger cell voltage decrease from 0.658 to 0.566 V with a 153.3 μV $hour^{-1}$ average decay than Nafion XL, which exhibited a cell voltage decrease from 0.626 to 0.543 V with a 138.3 μV $hour^{-1}$ average decay. It should be noted that the SPP-TFP-4.0-PVDF and SPP-TFP-4.0 cells had much smaller cell voltage decay rates than the Nafion NRE 211 and Nafion XL cells, indicating the chemical robustness of their membranes. Although the ohmic resistance of the SPP-TFP-4.0-PVDF cell varied somewhat during the test, the average increase that directly reflected the membrane degradation was 51.7 microhm·cm^2 $hour^{-1}$ (from 0.301 to 0.332 ohm·cm^2) for SPP-TFP-4.0-PVDF cell, which was substantially lower than that of the SPP-TFP-4.0 cell (80.0 microhm·cm^2 $hour^{-1}$; from 0.285 to 0.333 ohm·cm^2). Conversely, the ohmic resistance of the Nafion NRE 211 and Nafion XL cells increased more notably from 0.315

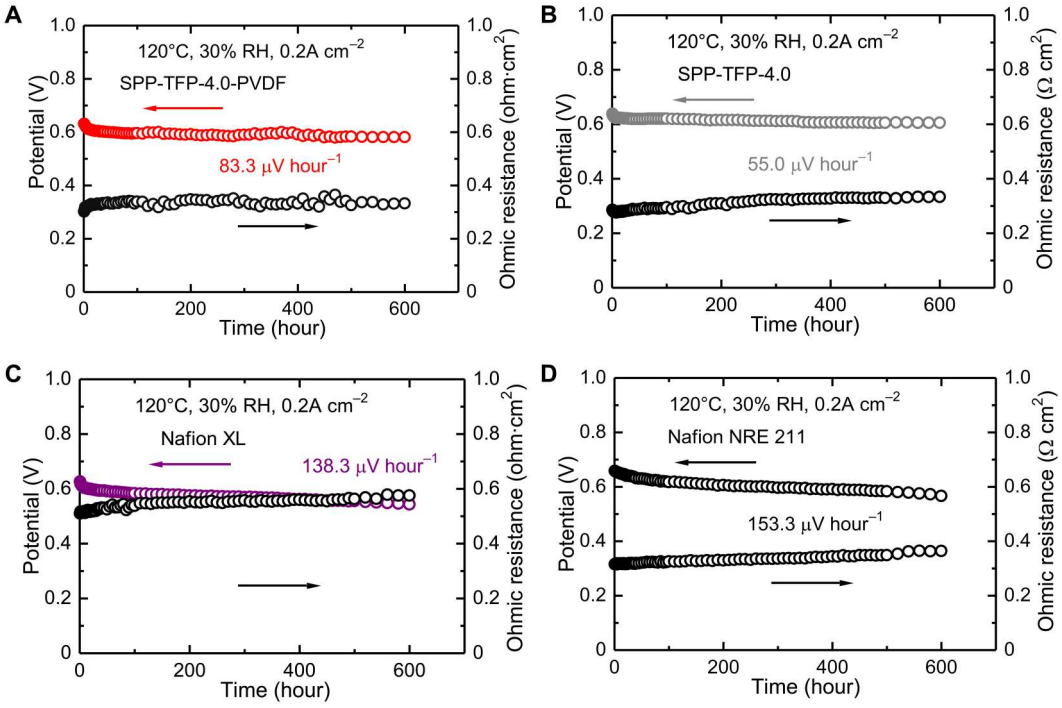

Fig. 5. Chemical stability at 120°C and 30% RH for 600 hours. (**A**) SPP-TFP-4.0-PVDF. (**B**) SPP-TFP-4.0. (**C**) Nafion XL. (**D**) Nafion NRE 211. The catalyst loading was 0.5 mg cm^{-2} for all electrodes supplying hydrogen (0.1 slpm) and air (0.1 slpm) to the anode and cathode, respectively, with no back pressure.

to 0.364 ohm·cm^2 (81.7 microhm·cm^2 $hour^{-1}$) and from 0.510 to 0.575 ohm·cm^2 (108.3 microhm·cm^2 $hour^{-1}$), respectively.

Combined chemical and mechanical durability at 90°C

Longevity is essential for the commercial application of alternative membranes. The DOE has established a technical target for membranes that will be used in automobile fuel cells in 2025. This target demands that membranes should survive over 20,000 cycles with a <20% OCV loss in an accelerated combined chemical (OCV hold) and mechanical (frequent wet/dry cycling) test (*6*). To the best of our knowledge, no reported PEMs (or MEAs) have reached the target. Here, the durability of the membranes was tested at 90°C while feeding H_2/air to the anode/cathode with dry (2 s) and wet (15 s) cycling to ensure that the difference in ohmic resistance between the dry and wet states was larger than 2.5 times. Except for SPP-TFP-4.0-ePTFE (wet/dry OCV: 0.82/0.79 V), all measured cells exhibited similar initial wet (0.91 V) and dry (0.86 to 0.87 V) OCVs (table S3). During the durability period, SPP-TFP-4.0, SPP-TFP-4.0-PVDF, SPP-TFP-4.0-ePTFE, Nafion NRE 211, and Nafion XL exhibited OCV losses of 20.9%/31.0%, 20.9%/25.2%, 12.2%/13.9%, 16.5%/29.1%, and 5.5%/64.0% at the wet/dry states, respectively. The OCV and ohmic resistance are plotted as functions of the number of humidity cycles and test duration (Fig. 6, A and B, and fig. S13). The parent SPP-TFP-4.0 (1173 cycles; 5.5 hours), SPP-TFP-4.0-ePTFE (233 cycles; 1.1 hours), and Nafion NRE 211 (8788 cycles; 41.5 hours) cells had short lifetimes and did not meet the DOE target. Among all cells, the SPP-TFP-4.0-PVDF cell exhibited the longest unprecedented lifetime of 148,870 cycles or 703.0 hours, which was 7.44 times longer than the DOE target and 1.69 times longer than that of the stabilized/reinforced Nafion XL (88,008 cycles or 415.6 hours). It is also noted that the OCV loss in the dry state was much smaller for the SPP-TFP-4.0-PVDF cell than that for the Nafion XL cell.

The CCMs were recovered after the test. As shown in fig. S14, the SPP-TFP-4.0 and SPP-TFP-4.0-ePTFE CCMs had noticeable cracks, while Nafion NRE 211 had visible pinholes (*50*), indicating that the tests were terminated because of mechanical failures. Contrarily, the SPP-TFP-4.0-PVDF and Nafion XL CCMs had no visible defects after the test. Thereafter, the recovered membranes were subjected to stress/stretching tests at 80°C and 60% RH (fig. S15 and table S4). Compared to the untested membranes (Fig. 3C), the posttest SPP-TFP-4.0-PVDF membranes exhibited only a 2.5% decrease in rupture energy, while Nafion XL exhibited 69.7 and 60.5% decreases in rupture energy in the MD and TD, respectively. The surface SEM images (fig. S16, A and B) revealed thin and minor cracks on the catalyst layer of posttest SPP-TFP-4.0-PVDF CCM and large and severe cracks on the catalyst layer of posttest Nafion XL CCM. As both CCMs used the same catalyst layers, the differences in the membranes affected the deformation of the anode catalyst layers. From the cross-sectional images (fig. S16, C and D), SPP-TFP-4.0-PVDF and Nafion XL both became slightly thinner (12 and 27 μm) than before (14 and 30 μm) with 2.8 and 7.2 nm $hour^{-1}$ thinning rate, respectively. The thinning would be caused by possible chemical degradation and long-term pressing in the cells. The SEM images revealed that there were minor cracks in the anode catalyst layer of SPP-TFP-4.0-PVDF CCM and more and larger cracks and defects throughout the anode catalyst layer of Nafion XL CCM. The chemical degradation of Nafion XL must have triggered the degradation of the Nafion binder in the anode.

Figure 6 (C and D) summarizes the relationship between changes in rupture energy (mechanical stability) and cell voltage

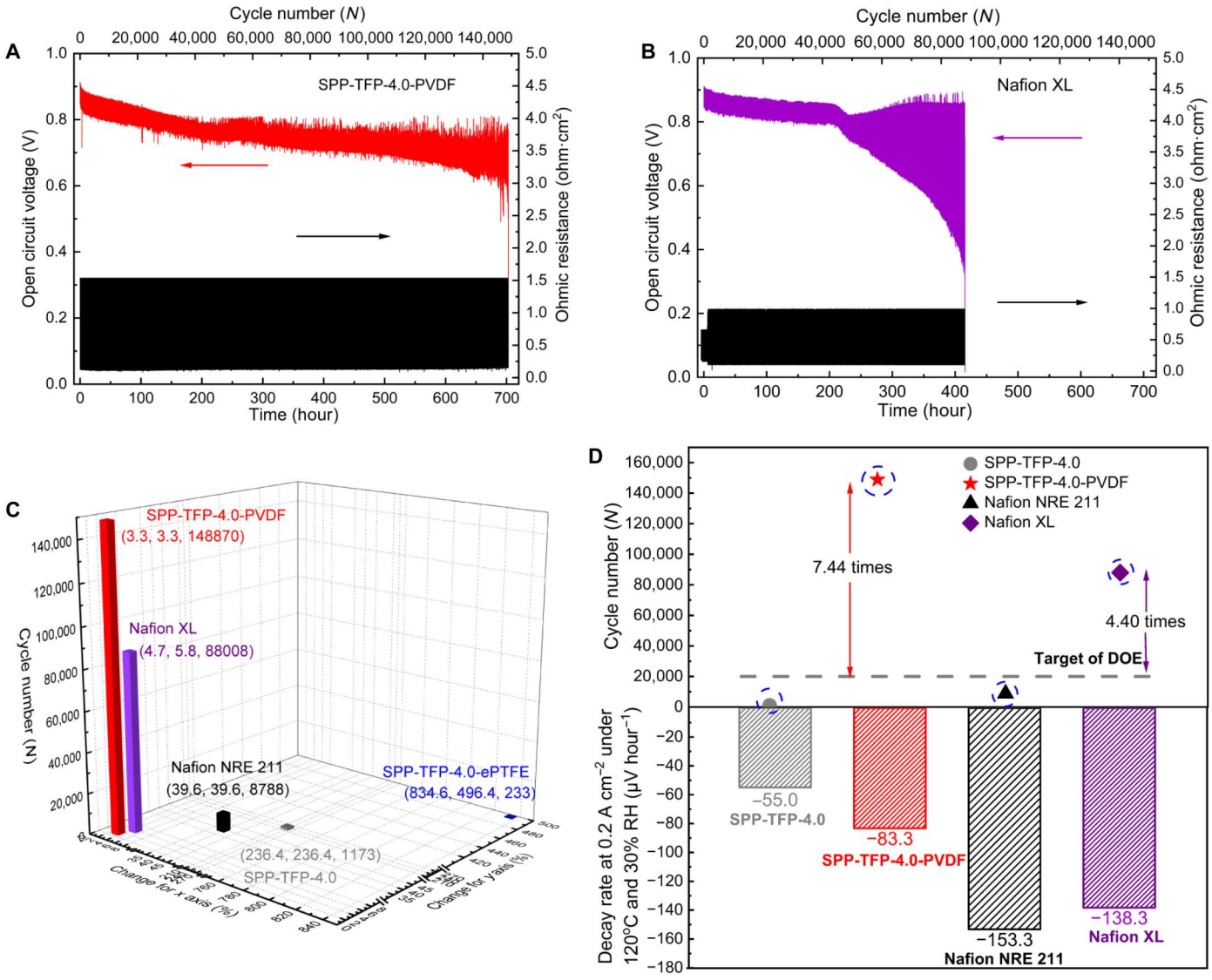

Fig. 6. Combined chemical (OCV hold) and mechanical (wet/dry cycling) durability at 90°C without backpressure. The test duration and cycle number dependence of the OCV and ohmic resistance of (**A**) SPP-TFP-4.0-PVDF and (**B**) Nafion XL. (**C**) The relationship between changes in rupture energy from 0 to 60% RH and the number of cycles in the combined chemical and mechanical durability test. The *x* axis is the change in rupture energy in the MD direction, the *y* axis is the change in rupture energy in the TD direction, and the *z* axis is the number of cycles in the combined chemical and mechanical durability test. (**D**) The relationship between decay rate (at 0.2 A cm^{-2}, 120°C, and 30% RH) and the number of cycles in the combined chemical and mechanical durability test. The catalyst loading was 0.2 and 0.1 mg cm^{-2} for the anode and cathode, respectively, feeding hydrogen (0.06 slpm, anode) and air (0.06 slpm, cathode). The measurement was subjected at OCV with frequent wet/dry cycling via switching wet gas (100% RH; 15 s) and dry gas (0% RH; 2 s).

decay rate (chemical stability) and the number of cycles survived in the combined chemical/mechanical durability test. The durability in the combined test decreased exponentially as the change in rupture energy and cell voltage decay increased. Therefore, stable (or nearly constant) rupture energy over a wide range of humidity and chemical robustness are two crucial parameters for enhancing the practical lifetime of membranes in operando fuel cells.

DISCUSSION

By the push-coating method, we successfully prepared sulfonated and fluorinated polyphenylene-based–reinforced membranes SPP-TFP-4.0-PVDF and SPP-TFP-4.0-ePTFE, comprising an SPP-TFP-4.0 ionomer and a porous nonwoven PVDF nanofiber fabric or an ePTFE substrate, respectively. The reinforced membranes effectively suppressed water uptake and swelling but exhibited higher proton conductivity than the commercial Nafion membrane. Compared to the reinforced SPP-TFP-4.0-ePTFE membrane, which exhibited large anisotropic properties in the TD and MD, the isotropic SPP-TFP-4.0-PVDF membrane showed the most stable mechanical properties from 0 to 60% RH at 80°C, with only a 3.3% change in rupture energy. In the same humidity range, Nafion NRE 211 exhibited a 39.6% decrease in rupture energy, while the chemically stabilized and physically reinforced Nafion XL

membrane exhibited 4.7 and 5.8% increases in rupture energy in the MD and TD, respectively. In addition, SPP-TFP-4.0-PVDF outperformed Nafion NRE 211 and Nafion XL by exhibiting outstanding fuel cell performance at high temperatures (100° to 120°C) without back pressure as well as minor in situ chemical degradation at 0.2 A cm^{-2}, 120°C, and 30% RH. In an ADT with frequent wet/dry cycling under OCV hold conditions, SPP-TFP-4.0-PVDF demonstrated a long lifetime (148,870 cycles and 703.0 hours), which is 7.44 times longer than the DOE target and 1.69 times longer than that of Nafion XL, as well as unprecedented durability for PEMs, including fluorinated, unfluorinated, and physically or chemically reinforced ones. This was because the tuned combination of SPP-TFP-4.0 ionomer and porous nonwoven PVDF fabric supported high proton-conducting properties, chemical and physical robustness of the composite SPP-TFP-4.0-PVDF membrane. The concept of stable rupture energy under a wide range of humidity will be further tested for a variety of ionomer membranes and porous substrates including less fluorinated and, thus, more environmentally benign materials. This discovery should usher in a next era of PEMFCs with high-temperature operability and durability for wider applications.

MATERIALS AND METHODS

Chemicals

The SPP-TFP-4.0 ionomer (M_n = 104 kDa; M_w = 556.1 kDa) was prepared using the same method reported in our previous paper (*50*). Nonwoven PVDF nanofiber fabric (fabricated by the mass production machine of LEMON COMPANY LIMITED) and ePTFE substrate were used as porous substrates, and their physical parameters are listed in table S5. The Nafion XL membrane, an anisotropic membrane mechanically reinforced with ePTFE, was purchased from Du Pont, and its MD and TD were indicated (*17*).

Preparation of the reinforced SPP-TFP-4.0-PVDF and SPP-TFP-4.0-ePTFE membranes

The reinforced SPP-TFP-4.0 membranes were fabricated using the push-coating method (fig. S17). To fabricate SPP-TFP-4.0-PVDF, a homogenous and degassed 12 weight % (wt %) isopropanol solution of SPP-TFP-4.0 was poured onto a flat glass plate and then spread over using a bar coater (slit width: 76.2 μm). Then, a porous PVDF fabric sheet was placed over the thin solution layer. An additional SPP-TFP-4.0 solution was poured and spread (slit width: 152.4 μm) over the PVDF sheet. Thereafter, the solution was covered with a thin silicone sheet (thickness: 1 mm) without including air bubbles. After drying for 15 hours at 25°C, a flexible and transparent reinforced SPP-TFP-4.0-PVDF membrane was peeled off from the glass plate and silicone sheet. Before the physical characterizations and property measurements, the SPP-TFP-4.0-PVDF membrane was successively treated with 1 M sulfuric acid and water to ensure that it was in an acidic (H^+) form.

Titration

The titrated IEC of the reinforced membranes was measured via acid-base titrations. At 50°C, a piece of the dried membrane was immersed in a 2 M NaCl aqueous solution for 48 hours to replace H^+ with Na^+ ions. A standard 0.01 M NaOH aqueous solution was used to titrate the released H^+ at room temperature.

Morphological characterization

The membrane samples (2 × 5 mm) wrapped with epoxy resin were smoothed and wrapped with conductive tape for SEM analysis. After sputtering with Pt, the cross-sectional images and elemental distribution of the samples were obtained using a Hitachi SU3500 device equipped with an EDS detector (Oxford Instruments) at an accelerating voltage of 15.0 kV. For TEM analysis, the membrane samples were stained with a 0.5 M $Pb(OAc)_2$ aqueous solution, washed with water, and dried. The stained membranes were embedded in epoxy resin, sectioned to 50 nm thickness with Leica microtome Ultracut UCT, and then placed on a copper grid. The TEM images were captured using the Hitachi H-9500 at an accelerating voltage of 200 kV.

Water uptake and proton conductivity

The water uptake and proton conductivity of the membranes were measured at 80°C and different RH levels using a polymer electrolyte analyzer (MSBAD-V-FC, Bel Japan Co.) equipped with a temperature- and humidity-controllable chamber. A magnetic suspension balance was used to measure the weight of the membranes. After vacuum-drying for 3 hours, the weight of the dried membrane (m_{dry}) was recorded, and the weight of the wet membrane (m_{wet}) was collected by exposing the membrane to the set humidity level. The water uptake of the membrane was calculated using the following equation: water uptake = $(m_{wet} - m_{dry}) \times 100/m_{dry}$. A four-probe conductivity cell equipped with a Solartron 1255B and SI1287 impedance analyzer was used to measure the proton conductivity (in millisiemens per centimeter) of the membranes using the following equation: $\sigma = l \times 1000/(A \times R)$, where l (in centimeters) is the length of the membrane between the two reference electrodes, A (in square centimeters) is the conducting area, and R (in ohms) is the ion-conductive resistance. The number of absorbed water molecules per sulfonic acid group (λ) = water uptake × 1000/(IEC × 18). The proton mobility μ_{H+} was calculated from the following equation (*34*): $\mu_{H+} = \sigma/(F \times IECv)$, where F is the Faraday constant and IECv is the volumetric IEC.

Mechanical properties

A Shimadzu AGS-J-500 N universal test machine equipped with a temperature- and humidity-controllable chamber was used to measure the tensile properties of the membrane samples. A membrane sample was cut into a dumbbell shape [35 × 6 mm (total) and 12 × 2 mm (test area)]. The stress-strain curves were obtained at 80°C and 0 or 60% RH at a stretching rate of 10 mm min^{-1} after equilibrating the sample at least for 3 hours. The rupture energy was obtained from the integral area of the stress and strain curves. An ITK DVA-225 dynamic mechanical analyzer was used to evaluate the viscoelastic properties of the samples at 80°C. The humidity dependence of E′, E″, and tan δ was measured at 80°C from 0 to 90% RH at a humidifying rate of 1% RH min^{-1}. Temperature dependence of E′, E″, and tan δ was measured at 60% RH from room temperature to 95°C at a heating rate of 1°C min^{-1}.

MEA preparation

A well-dispersed catalyst ink was prepared by mixing commercial Pt/carbon black (46.3%Pt; TEC10E50E, Tanaka Kikinzoku Kogyo K.K.), a 5 wt % Nafion ionomer solution (IEC = 0.95 to 1.03 mmol g^{-1}; D521, DuPont), ethanol, and deionized water via ball-milling. The Nafion ionomer to carbon-support mass ratio was

0.7. CCMs were fabricated by spraying the catalyst ink onto both sides of the membranes using a Nordson pulse-swirl-spray apparatus. The obtained CCMs were dried in an oven at 60°C for 12 hours, and then hot-pressed at 140°C and 1 MPa for 3 min. The Pt loading amounts in the catalyst layer and geometric area were 0.5 ± 0.03 mg cm^{-2} (each electrode) and 4.41 cm^2, respectively. The CCMs were sandwiched by two gas diffusion layers (29 BC, carbon paper; SGL Group) and mounted into a cell.

Fuel cell performance

An assembled MEA was mounted into a single fuel cell hardware. After checking the air-tightness, the cell was set into the fuel cell evaluation station (FCE-1, Panasonic Production Technology) equipped with an electronic load (PLZ-664WA, Kikusui Denshi) and a digital AC milliohmmeter (1 kHz; Model 3566, Tsuruga Denki). All operations were carried out without back pressure. The initial conditioning of the cells was conducted as follows. The temperature and humidity were set at 40°C and 100% RH, respectively, supplying nitrogen [0.1 slpm (standard liters per minute)] to both electrodes (>2 hours). After changing the anode flow gas to hydrogen (0.1 slpm) for 30 min, oxygen (0.1 slpm) was fed to the cathode for 5 min. The cell was discharged from 0.02 to 1 A cm^{-2}, where the equilibration time was 3 min at each current density. After discharging at 1, 0.75, and 0.2 A cm^{-2} for 1 hour, respectively, the current density was set at 0 A cm^{-2} (OCV). Simultaneously, the feeding gas to the cathode was changed to nitrogen (0.1 slpm). After the cell voltage decreased lower than 0.1 V, the cathode was cleaned by CV. The potential was swept from 0.075 to 1.0 V versus RHE (reversible hydrogen electrode) at a scan rate of 20 mV s^{-1} for 50 cycles. The ECSA was calculated according to the literature (*56*). The temperature and humidity were set at 80°C and 100% RH, respectively, equilibrating for >2 hours. Then, linear sweep voltammetry was conducted at 80°C and 100% RH to evaluate the hydrogen permeability of the membranes from the anode to the cathode. The linear sweep voltammogram was measured by sweeping the potential from 0.15 to 0.6 V at a scan rate of 0.5 mV s^{-1}, supplying hydrogen (0.1 slpm, anode) and nitrogen (0.1 slpm, cathode). The hydrogen crossover current density was obtained by averaging the value from 0.25 to 0.5 V. Taking into account the thickness, the hydrogen permeability was calculated according to the literature (*53*), where the related equation was P (permeability coefficient) = i (crossover current density) × thickness/4 × F (Faraday constant). Then, the fuel cell performance was evaluated from the polarization curves, feeding hydrogen, and air to the anode and cathode, respectively. The test procedure was as follows. After the activation at 0.2 A cm^{-2} for 2 hours, the current density slowly decreased to 0 A cm^{-2}. The *IV* measurement was conducted and repeated three times, where the current density was increased from 0 to 1.5 A cm^{-2}, supplying hydrogen (from 0.02 to 0.066 slpm, 70% gas utilization of hydrogen) to the anode and supplying air (from 0.08 to 0.274 slpm, 40% gas utilization of air) to the cathode. For example, the hydrogen flow rate was 0.036 and 0.044 slpm at 0.8 and 1.0 A cm^{-2}, respectively. The air flow rate was 0.147 and 0.183 slpm at 0.8 and 1.0 A cm^{-2}, respectively. The *IV* data were stopped to record when the current density became higher than 1.5 A cm^{-2} or the cell voltage became lower than 0.3 V. Then, the performance was measured in the order of 80°C and 30% RH, 100°C and 53% RH, 100°C and 30% RH, and 120°C and 30% RH, where the conditions were equilibrated for more than 6 hours before each measurement. The EIS was obtained from 5 kHz to 0.01 Hz at 0.1 A cm^{-2}, 80°C, 100% RH with no backpressure, supplying hydrogen (0.1 slpm) and air (0.1 slpm) to the anode and cathode, respectively.

Stability test at a constant current density (0.2 A cm^{-2}), 120°C, and 30% RH

After the aforementioned activation, cleaning, and linear sweep voltammetry measurements, the temperature and humidity of the cell were changed to 120°C and 30% RH, and the cell was equilibrated for more than 12 hours. Then, the stability of the fuel cell was measured at a constant current density (0.2 A cm^{-2}), supplying hydrogen (0.1 slpm) and air (0.1 slpm) to the anode and cathode, respectively. The stability test was carried out with no back pressure. The prepared CCM for this test was the same as that for the fuel cell performance test. The Pt loading amount in the catalyst layer was 0.5 ± 0.03 mg cm^{-2} (both electrodes).

Combined chemical (OCV hold) and mechanical (wet/dry cycling) durability test

A combined chemical and mechanical durability test was performed in accordance with the DOE protocol (*6*) and our previous study (*46*). A CCM was prepared in a similar manner as described above, except that the Pt loading amounts in the anode and cathode were 0.2 ± 0.02 and 0.1 ± 0.03 mg cm^{-2}, respectively. The measurement was conducted at 90°C and OCV conditions while supplying hydrogen (0.06 slpm) to the anode and air (0.06 slpm) to the cathode, with frequent wet/dry cycling via switching wet gas (100% RH; 15 s) and dry gas (0% RH; 2 s) with no backpressure.

Supplementary Materials

This PDF file includes:

Figs. S1 to S17
Tables S1 to S5

REFERENCES AND NOTES

1. Z. P. Cano, D. Banham, S. Ye, A. Hintennach, J. Lu, M. Fowler, Z. Chen, Batteries and fuel cells for emerging electric vehicle markets. *Nat. Energy* **3**, 279–289 (2018).
2. I. Staffell, D. Scamman, A. Velazquez Abad, P. Balcombe, P. E. Dodds, P. Ekins, N. Shah, K. R. Ward, The role of hydrogen and fuel cells in the global energy system. *Energ. Environ. Sci.* **12**, 463–491 (2019).
3. K. Jiao, J. Xuan, Q. Du, Z. Bao, B. Xie, B. Wang, Y. Zhao, L. Fan, H. Wang, Z. Hou, S. Huo, N. P. Brandon, Y. Yin, M. D. Guiver, Designing the next generation of proton-exchange membrane fuel cells. *Nature* **595**, 361–369 (2021).
4. A. G. Olabi, T. Wilberforce, M. A. Abdelkareem, Fuel cell application in the automotive industry and future perspective. *Energy* **214**, 118955–118973 (2021).
5. M. Miotti, J. Hofer, C. Bauer, Integrated environmental and economic assessment of current and future fuel cell vehicles. *Int. J. Life Cycle Assess* **22**, 94–110 (2017).
6. Fuel cell Technical Team Roadmap (2017); www.energy.gov/eere/vehicles/downloads/us-drive-fuel-cell-technical-team-roadmap.
7. Y.-H. Lai, K. M. Rahmoeller, J. H. Hurst, R. S. Kukreja, M. Atwan, A. J. Maslyn, C. S. Gittleman, Accelerated stress testing of fuel cell membranes subjected to combined mechanical/chemical stressors and cerium migration. *J. Electrochem. Soc.* **165**, F3217–F3229 (2018).
8. L. Ghassemzadeh, T. J. Peckham, T. Weissbach, X. Luo, S. Holdcroft, Selective formation of hydrogen and hydroxyl radicals by electron beam irradiation and their reactivity with perfluorosulfonated acid ionomer. *J. Am. Chem. Soc.* **135**, 15923–15932 (2013).
9. M. Zatoń, J. Rozière, D. J. Jones, Current understanding of chemical degradation mechanisms of perfluorosulfonic acid membranes and their mitigation strategies: A review. *Sustain. Energy Fuels* **1**, 409–438 (2017).

10. M. Robert, A. El Kaddouri, J.-C. Perrin, K. Mozet, M. Daoudi, J. Dillet, J.-Y. Morel, S. André, O. Lottin, Effects of conjoint mechanical and chemical stress on perfluorosulfonic-acid membranes for fuel cells. *J. Power Sources* **476**, 228662–228672 (2020).
11. M. Breitwieser, C. Klose, A. Hartmann, A. Büchler, M. Klingele, S. Vierrath, R. Zengerle, S. Thiele, Cerium oxide decorated polymer nanofibers as effective membrane reinforcement for durable, high-performance fuel cells. *Adv. Energy Mater.* **7**, 1602100–1602109 (2016).
12. S.-H. Shin, A. Kodir, D. Shin, S.-H. Park, B. Bae, Perfluorinated composite membranes with organic antioxidants for chemically durable fuel cells. *Electrochim. Acta* **298**, 901–909 (2019).
13. X. Liu, Y. Li, M. Li, N. Xie, J. Zhang, Y. Qin, Y. Yin, M. D. Guiver, Durability enhancement of proton exchange membrane fuel cells by ferrocyanide or ferricyanide additives. *J. Membr. Sci.* **629**, 119282–119294 (2021).
14. C.-K. Hwang, K. A. Lee, J. Lee, Y. Kim, H. Ahn, W. Hwang, B.-K. Ju, J. Y. Kim, S. Y. Yeo, J. Choi, Y.-E. Sung, I.-D. Kim, K. R. Yoon, Perpendicularly stacked array of PTFE nanofibers as a reinforcement for highly durable composite membrane in proton exchange membrane fuel cells. *Nano Energy* **101**, 107581–107592 (2022).
15. J. Park, L. Wang, S. G. Advani, A. K. Prasad, Durability analysis of Nafion/hydrophilic pretreated PTFE membranes for PEMFCs. *J. Electrochem. Soc.* **159**, F864–F870 (2012).
16. J.-E. Cha, S. Jang, D.-J. Seo, J. Hwang, M. H. Seo, Y.-W. Choi, W. B. Kim, A reinforced composite membrane of two-layered asymmetric structure with Nafion ionomer and polyethylene substrate for improving proton exchange membrane fuel cell performance. *Chem. Eng. J.* **454**, 140091–140102 (2023).
17. M. Han, Y.-G. Shul, H. Lee, D. Shin, B. Bae, Accelerated testing of polymer electrolyte membranes under open-circuit voltage conditions for durable proton exchange membrane fuel cells. *Int. J. Hydrogen Energy* **42**, 30787–30791 (2017).
18. S. Shi, A. Z. Weber, A. Kusoglu, Structure/property relationship of Nafion XL composite membranes. *J. Membr. Sci.* **516**, 123–134 (2016).
19. W. Liu, T. Suzuki, H. Mao, T. Schmiedel, Development of thin, reinforced PEMFC membranes through understanding of structure-property-performance relationships. *ECS Trans.* **50**, 51–64 (2013).
20. B. Kienitz, J. Kolde, S. Priester, C. Baczkowski, M. Crum, Ultra-thin reinforced ionomer membranes to meet next generation fuel cell targets. *ECS Trans.* **41**, 1521–1530 (2011).
21. P. M. Ngo, H. Nakajima, T. Karimata, T. Saitou, K. Ito, Investigation of in-situ catalytic combustion in polymer-electrolyte-membrane fuel cell during combined chemical and mechanical stress test. *J. Power Sources* **542**, 231803–231813 (2022).
22. A. Sadeghi Alavijeh, M. A. Goulet, R. M. H. Khorasany, J. Ghataurah, C. Lim, M. Lauritzen, E. Kjeang, G. G. Wang, R. K. N. D. Rajapakse, Decay in mechanical properties of catalyst coated membranes subjected to combined chemical and mechanical membrane degradation. *Fuel Cells* **15**, 204–213 (2015).
23. H. L. Nguyen, J. Han, X. L. Nguyen, S. Yu, Y.-M. Goo, D. D. Le, Review of the durability of polymer electrolyte membrane fuel cell in long-term operation: Main influencing parameters and testing protocols. *Energies* **14**, 4048–4082 (2021).
24. N. S. Khattra, M. E. Hannach, K. H. Wong, M. Lauritzen, E. Kjeang, Estimating the durability of polymer electrolyte fuel cell membranes using a fracture percolation model. *J. Electrochem. Soc.* **167**, 013528 (2019).
25. M. Robert, A. El Kaddouri, J. C. Perrin, K. Mozet, J. Dillet, J. Y. Morel, O. Lottin, The impact of chemical-mechanical ex situ aging on PFSA membranes for fuel cells. *Membranes* **11**, 366–375 (2021).
26. S. H. Shin, P. J. Nur, A. Kodir, D. H. Kwak, H. Lee, D. Shin, B. Bae, Improving the mechanical durability of short-side-chain perfluorinated polymer electrolyte membranes by annealing and physical reinforcement. *ACS Omega* **4**, 19153–19163 (2019).
27. J. Zhao, X. Li, A review of polymer electrolyte membrane fuel cell durability for vehicular applications: Degradation modes and experimental techniques. *Energ. Conver. Manage.* **199**, 112022–112044 (2019).
28. R. Mukundan, A. M. Baker, A. Kusoglu, P. Beattie, S. Knights, A. Z. Weber, R. L. Borup, Membrane accelerated stress test development for polymer electrolyte fuel cell durability validated using field and drive cycle testing. *J. Electrochem. Soc.* **165**, F3085–F3093 (2018).
29. T. J. Skalski, B. Britton, T. J. Peckham, S. Holdcroft, Structurally-defined, sulfo-phenylated, oligophenylenes and polyphenylenes. *J. Am. Chem. Soc.* **137**, 12223–12226 (2015).
30. J. Miyake, R. Taki, T. Mochizuki, R. Shimizu, R. Akiyama, M. Uchida, K. Miyatake, Design of flexible polyphenylene proton-conducting membrane for next-generation fuel cells. *Sci. Adv.* **3**, eaao0476 (2017).
31. N. R. Kang, T. H. Pham, P. Jannasch, Polyaromatic perfluorophenylsulfonic acids with high radical resistance and proton conductivity. *ACS Macro Lett.* **8**, 1247–1251 (2019).
32. M. Adamski, N. Peressin, S. Holdcroft, On the evolution of sulfonated polyphenylenes as proton exchange membranes for fuel cells. *Mater. Adv.* **2**, 4966–5005 (2021).
33. Z. Long, K. Miyatake, High-performance fuel cell operable at 120°C using polyphenlyene ionomer membranes with improved interfacial compatibility. *ACS Appl. Mater. Interfaces* **13**, 15366–15372 (2021).
34. M. Adamski, T. J. G. Skalski, B. Britton, T. J. Peckham, L. Metzler, S. Holdcroft, Highly stable, low gas crossover, proton-conducting phenylated polyphenylenes. *Angew. Chem. Int. Ed.* **56**, 9058–9061 (2017).
35. C. S. Gittleman, H. Jia, E. S. De Castro, C. R. I. Chisholm, Y. S. Kim, Proton conductors for heavy-duty vehicle fuel cells. *Joule* **5**, 1660–1677 (2021).
36. S. Xu, Y. Wu, M. Adamski, K. Fraser, S. Holdcroft, Understanding the role of acid–base interactions using architecturally-controlled, pyridyl-bearing sulfonated phenylated polyphenylenes. *J. Mater. Chem. A* **8**, 23866–23883 (2020).
37. J. Miyake, T. Watanabe, H. Shintani, Y. Sugawara, M. Uchida, K. Miyatake, Reinforced polyphenylene ionomer membranes exhibiting high fuel cell performance and mechanical durability. *ACS Mater. Au* **1**, 81–88 (2021).
38. Z. Shang, M. M. Hossain, R. Wycisk, P. N. Pintauro, Poly(phenylene sulfonic acid)-expanded polytetrafluoroethylene composite membrane for low relative humidity operation in hydrogen fuel cells. *J. Power Sources* **535**, 231375–231383 (2022).
39. Z. Long, K. Miyatake, ePTFE reinforced, sulfonated aromatic polymer membranes enable durable, high-temperature operable PEMFCs. *iScience* **24**, 102962–102977 (2021).
40. H. Nguyen, C. Klose, L. Metzler, S. Vierrath, M. Breitwieser, Fully hydrocarbon membrane electrode assemblies for proton exchange membrane fuel cells and electrolyzers: An engineering perspective. *Adv. Energy Mater.* **12**, 2103559–2103578 (2022).
41. B. Yuan, K. Wen, D. Chen, Y. Liu, Y. Dong, C. Feng, Y. Han, J. Han, Y. Zhang, C. Xia, A. Sun, W. He, Composite separators for robust high rate lithium ion batteries. *Adv. Funct. Mater.* **31**, 2101420–2101469 (2021).
42. R. Prasanth, N. Shubha, H. H. Hng, M. Srinivasan, Effect of poly(ethylene oxide) on ionic conductivity and electrochemical properties of poly(vinylidenefluoride) based polymer gel electrolytes prepared by electrospinning for lithium ion batteries. *J. Power Sources* **245**, 283–291 (2014).
43. G. Zainab, X. Wang, J. Yu, Y. Zhai, A. Ahmed Babar, K. Xiao, B. Ding, Electrospun polyacrylonitrile/polyurethane composite nanofibrous separator with electrochemical performance for high power lithium ion batteries. *Mater. Chem. Phys.* **182**, 308–314 (2016).
44. R. Sood, S. Cavaliere, D. J. Jones, J. Rozière, Electrospun nanofibre composite polymer electrolyte fuel cell and electrolysis membranes. *Nano Energy* **26**, 729–745 (2016).
45. S. N. Banitaba, A. Ehrmann, Application of electrospun nanofibers for fabrication of versatile and highly efficient electrochemical devices: A review. *Polymers* **13**, 1741–1782 (2021).
46. S. Cavaliere, S. Subianto, I. Savych, D. J. Jones, J. Rozière, Electrospinning: Designed architectures for energy conversion and storage devices. *Energ. Environ. Sci.* **4**, 4761–4785 (2011).
47. C. Zhu, T. Nagaishi, J. Shi, H. Lee, P. Y. Wong, J. Sui, K. Hyodo, I. S. Kim, Enhanced wettability and thermal stability of a novel polyethylene terephthalate-based poly(vinylidene fluoride) nanofiber hybrid membrane for the separator of lithium-ion batteries. *ACS Appl. Mater. Interfaces* **9**, 26400–26406 (2017).
48. Y. Li, J. Hui, J. Kawchuk, A. O'Brien, Z. Jiang, M. Hoorfar, Composite membranes of PVDF nanofibers impregnated with Nafion for increased fuel concentrations in direct methanol fuel cells. *Fuel Cells* **19**, 43–50 (2019).
49. J. Woo Park, R. Wycisk, G. Lin, P. Ying Chong, D. Powers, T. Van Nguyen, R. P. Dowd Jr., P. N. Pintauro, Electrospun Nafion/PVDF single-fiber blended membranes for regenerative H2/Br2 fuel cells. *J. Membr. Sci.* **541**, 85–92 (2017).
50. F. H. Liu, K. Miyatake, Well-designed polyphenylene PEMs with high proton conductivity and chemical and mechanical durability for fuel cells. *J. Mater. Chem. A* **10**, 7660–7667 (2022).
51. M. A. Hickner, H. Ghassemi, Y. S. Kim, B. R. Einsla, J. E. McGrath, Alternative polymer systems for proton exchange membranes (PEMs). *Chem. Rev.* **104**, 4587–4612 (2004).
52. C. Y. Wong, W. Y. Wong, K. Ramya, M. Khalid, K. S. Loh, W. R. W. Daud, K. L. Lim, R. Walvekar, A. A. H. Kadhum, Additives in proton exchange membranes for low- and high-temperature fuel cell applications: A review. *Int. J. Hydrogen Energy* **44**, 6116–6135 (2019).
53. Y. S. Kim, K.-S. Lee, Fuel cell membrane characterizations. *Polym. Rev.* **55**, 330–370 (2015).
54. F. Akitomo, T. Sasabe, T. Yoshida, H. Naito, K. Kawamura, S. Hirai, Investigation of effects of high temperature and pressure on a polymer electrolyte fuel cell with polarization analysis and X-ray imaging of liquid water. *J. Power Sources* **431**, 205–209 (2019).
55. E. Endoh, Development of highly durable PFSA membrane and MEA for PEMFC under high temperature and low humidity conditions. *ECS Trans.* **16**, 1229–1240 (2008).
56. Q. Zhang, S. Dong, P. Shao, Y. Zhu, Z. Mu, D. Sheng, T. Zhang, X. Jiang, R. Shao, Z. Ren, J. Xie, X. Feng, B. Wang, Covalent organic framework-based porous ionomers for high-performance fuel cells. *Science* **378**, 181–186 (2022).

Acknowledgments: We thank the Valqua LTD company for the provided ePTFE substrate. **Funding:** This work was partly supported by the New Energy and Industrial Technology Development Organization (NEDO), the Ministry of Education, Culture, Sports, Science and Technology (MEXT), Japan, through Grants-in-Aid for Scientific Research (18H05515 and 23H02058) and MEXT Program: Data Creation and Utilization Type Material Research and Development Project (JPMXP1122712807), JKA promotion funds from AUTORACE, and the China Scholarship Council (CSC). **Author contributions:** K.M. developed the intellectual concept and supervised this research. I.S.K. designed and prepared porous PVDF nanofiber fabric. F.L. designed and performed the experiments. F.L. and K.M. analyzed all the experimental data and wrote the paper. **Competing interests:** The authors declare that they have no competing interests. **Data and materials availability:** All data needed to evaluate the conclusions in the paper are present in the paper and/or the Supplementary Materials.

Submitted 29 January 2023
Accepted 23 June 2023
Published 26 July 2023
10.1126/sciadv.adg9057